Journal of Applied Electrochemistry **29**: 813–820, 1999.
© 1999 *Kluwer Academic Publishers. Printed in the Netherlands.*

Influence of Co^{2+} and Mn^{2+} ions on the kinetics of lead anodes for zinc electrowinning

C. CACHET, C. LE PAPE-RÉROLLE and R. WIART
UPR 15 du CNRS, Physique des Liquides et Électrochimie, Université Pierre et Marie Curie, Tour 22, 4 Place Jussieu, 75252 Paris Cedex 05, France

Received 2 April 1998; accepted in revised form 1 December 1998

Key words: cobalt ions, impedance spectroscopy, lead anode, manganese ions, zinc electrowinning

Abstract

The influence of Co^{2+} and Mn^{2+} ions on the kinetics of lead and lead–silver alloy anodes is analysed using impedance spectroscopy and steady-state polarisation curves. With lead–silver anodes, increasing the Mn^{2+} concentration catalyses the oxygen evolution current by stimulating the reaction rate. Impedance data reveal a transient inhibition of the reaction, ascribed to the adsorption of a silver-salt containing manganese. The addition of Co^{2+} catalyses oxygen evolution, mainly on the pure lead anode. For lead–silver anodes, the small catalytic effect of Co^{2+} ions implies an increase in the Tafel coefficient for the oxygen reaction. The transient inhibiting process suggests the formation of a cobalt-containing adsorbate on the pure lead anode.

1. Introduction

The influence of Co^{2+} ions on zinc electrowinning has been extensively investigated, essentially on the cathodic process of zinc deposition [1–12], which is strongly affected by the presence in the electrolytes of metal impurities more electropositive than zinc. From measurements of the induction time, prior to electrolysis destabilization, these impurities have been classified with respect to their deleterious effect on zinc deposition, which decreases in the order Ge, Sb, Ni, Co, Bi, Cu, As, Sn, Fe [7]. From impedance measurements, it has been shown that hydrogen evolution is enhanced by adsorbed Co^{2+} ions, thus inducing the redissolution of the zinc deposit observable from the potential dependencies of current, charge transfer resistance and double layer capacitance [13].

Other work has been devoted to the influence of cobalt on the lead anode, and this element appears to be beneficial in zinc electrowinning. It has been shown that both Co in the Pb–Co alloy and Co^{2+} in the electrolyte are able to reduce the anodic potential for oxygen evolution and increase the corrosion resistance of lead anodes [14–17]. The catalytic effect of cobalt has been attributed to a lowering of oxygen overpotential through the reaction [18]:

$$Co^{2+} = Co^{3+} + e^-$$

and

$$4\,Co^{3+} + 2\,H_2O = 4\,Co^{2+} + 4\,H^+ + O_2$$

or

$$2\,Co^{3+} + 2\,H_2O = H_2O_2 + 2\,Co^{2+} + 2\,H^+$$

$$2\,H_2O_2 = 2\,H_2O + O_2$$

It has been shown that the addition of Co^{2+} to the electrolyte retards the formation of PbO_2 as a corrosion product, and decreases the Tafel slope from 120 mV to 62–68 mV, which indicates a catalytic effect on oxygen evolution.

Silver in lead anodes and Mn^{2+} ions in solution are used in zinc electrowinning because they decrease both the oxygen overpotential [19–21] and the anode corrosion rate [19, 20, 22–25]. During zinc electrowinning in Co-free electrolytes, impedance spectroscopy has already given indications about the kinetics of lead and lead–silver anodes [25–29]. For lead–silver anodes, and mainly with Mn^{2+} in the electrolyte, a transient inhibition process has been observed at the same time as

the catalytic effect on the steady-state current for oxygen evolution, thus revealing a complicated reaction mechanism in which two electrochemical processes compete in opposite directions on the electrode surface.

To date, no work has been carried out by impedance spectroscopy to investigate the reaction mechanism of oxygen evolution on lead or lead–silver anodes in the presence of Co^{2+} ions in the electrolyte. The aim of the present study was to use impedance spectroscopy to determine the influence of Co^{2+} ions on the kinetics of lead and lead–silver alloy anodes, polarised in electrolytes with and without Mn^{2+} ions. An attempt was also made to clarify the influence of the Mn^{2+} concentration on the electrode kinetics.

2. Experimental details

2.1. *Electrodes and cell*

Pure lead (Johnson Matthey, specpure 99.9999%) and silver–lead alloys (Union-Minière, silver content 0.56%, other impurities given Table 1) were used as anodes, with an effective surface area of 1.13 or 1 cm^2, respectively. These were vertically oriented in the cell. The counter electrode was aluminium (Union-Minière), with an effective surface area of 1 cm^2, positioned in front of the working electrode surface. All potentials are referred to the Hg/Hg_2SO_4 electrode (SSE).

Magnetic stirring of the electrolyte was carried out and the electrolysis cell, containing approximately 200 cm^3 of solution, was thermostated at 37 °C.

2.2. *Electrolytes*

The composition of the base electrolyte was 55 g dm^{-3} Zn^{2+} (as $ZnSO_4{\cdot}7H_2O$) and 180 g dm^{-3} H_2SO_4. The influence of Mn^{2+} and Co^{2+} ions was investigated by adding to the base electrolyte from 1 to 100 g dm^{-3} Mn^{2+} (as $MnSO_4.H_2O$) and 10 mg dm^{-3} Co^{2+} (as $CoSO_4.7H_2O$), respectively. All chemicals were Merck products of analytical purity.

Table 1. Impurity contents in Pb–Ag alloy (Union-Minière)

Impurity	ppm
Bi	<250
As	<1
Sn	<1
Fe	<8
Cu	<12
Sb	<1
Zn	<5
Cd	<10

2.3. *Experimental methods*

Potentiostatic polarization curves were obtained by potential steps of 20 mV, starting from a potential of 1.16 V or 1.3 V vs SSE for lead–silver or pure lead anodes, respectively. At each potential, V, current stabilization was obtained for a time of 15 min. At each steady-state point on the polarization curves, impedance measurements were made using a frequency response analyser (Solartron 1250) and an electrochemical interface (Solartron 1286) controlled by an IBM PS/2 microcomputer, by superimposing a 10 mV r.m.s. sine wave onto the direct potential. The steady-state polarization curves, $i(E)$, where i is the current density, were corrected for the ohmic drop, $R_e i = V - E$, the electrolyte resistance R_e being given by the high-frequency limit of the electrode impedance.

3. Results and discussion

3.1. *Case of lead–silver alloy anode*

Figure 1 presents the polarization curves, obtained with Pb–Ag anodes, polarized in the base electrolyte for various Mn^{2+} concentrations. The presence of Mn^{2+} ions in solution decreases the anode polarization. Such a catalytic effect is more pronounced with increasing Mn^{2+} concentration, up to a saturation limit observed between 5 and 10 g dm^{-3} Mn^{2+}.

The impedance plots obtained at low potentials along the polarization curves of Figure 1 mainly give, in the studied frequency domain and whatever the Mn^{2+} ions concentration, a high-frequency capacitive loop corresponding to the charge transfer resistance, R_t, of oxygen evolution in parallel with the double layer capacitance, C_{dl}. As examples, the plots obtained at $E = 1.2$ V, for the base electrolyte and the 10 g dm^{-3} Mn^{2+}-containing electrolyte, are presented in Figure 2(A) and (D), respectively. The high values of the double layer capacity, $C_{dl} > 3.5$ mF cm^{-2}, indicate that oxygen evolution probably takes place on a porous deposit of PbO_2, or $PbO_2 + MnO_2$ in Mn^{2+}-containing electrolyte [27, 28].

In Figure 3, the impedance plots obtained at $E = 1.355$ V are shown for the base electrolyte at point A′ and for the electrolytes containing 1, 5 or 10 g dm^{-3} Mn^{2+} ions, at points (B′), (C′) and (D′), respectively. For the base electrolyte, the impedance plot still gives a flattened capacitive loop. By contrast, for the Mn^{2+}-containing electrolytes, an additional medium-frequency capacitive loop with resistance R_o appears, corresponding to the transient inhibition process which

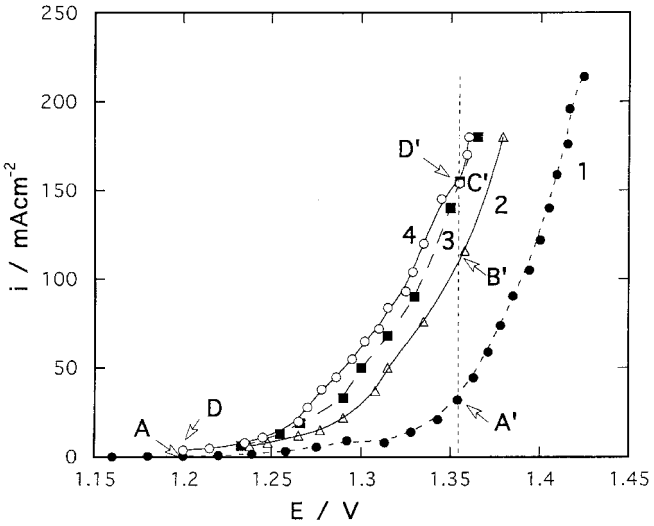

Fig. 1. Curves $i(E)$ obtained with Pb–Ag anodes polarized in the base electrolyte (curve 1), and in the same electrolyte containing various concentrations of Mn^{2+} ions: 1 g dm^{-3} (curve 2), 5 g dm^{-3} (curve 3) and 10 g dm^{-3} (curve 4).

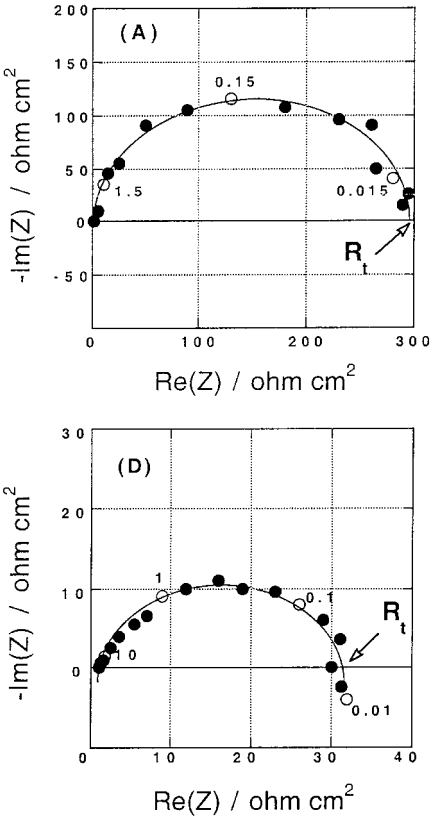

Fig. 2. Impedance plots obtained at $E = 1.2$ V in the base electrolyte (A), and in the same electrolyte containing 10 g dm^{-3} Mn^{2+} ions (D).

becomes more pronounced with increasing Mn^{2+} concentration. For 10 g dm^{-3} Mn^{2+} ions, a negative resistance appears, R_o, on plot D′, indicating much stronger inhibition at the electrode surface. A low-frequency inductive loop can also be seen on all diagrams in Figure 3. No changes are observed on the plots obtained for Mn^{2+} concentrations higher than 10 g dm^{-3}.

As already described [26, 27], the main reaction is that of oxygen evolution on a PbO_2/MnO_2 layer, since the partial current for the Mn^{2+} oxidation remains very low (about 1 mA cm^{-2}) in comparison with the total current. Consequently, in all the impedance diagrams, the high frequency capacitive loop is due to the charge transfer resistance of oxygen evolution in parallel with the double layer capacitance. The medium-frequency capacitive feature corresponds to the relaxation of the electrode coverage by an absorbed silver salt from a secondary reaction. In the presence of Mn^{2+} ions, this last reaction forms a silver salt ($AgMnO_4^-$) on the MnO_2 layer. The low-frequency inductive loop has been ascribed to the very slow relaxation of the conductivity of a sublayer of PbO present in the oxide layer.

These results confirm that the presence of Mn^{2+} ions in the electrolyte generates two opposite effects: a catalytic effect on steady-state polarization curves due to a stimulated rate constant of oxygen evolution on the MnO_2 layer, and a transient inhibition process. These two opposite effects become more pronounced with increasing Mn^{2+} concentration. Furthermore, when a strong transient inhibition (with a negative resistance) appears on the impedance plots, the catalytic effect on polarization curves attains saturation, which suggests that no more sites for oxygen evolution can be activated on the electrode surface.

The effect of Mn^{2+} ions on the kinetics of lead–silver alloy anodes remains prevalent in the presence of Co^{2+} ions. As shown in Figure 4, with the Mn^{2+}-containing electrolyte, there is no influence of Co^{2+} ions on the electrode potential, (curves 3 and 4), whereas a slight decrease in polarization (about 15 mV) is observed in the absence of Mn^{2+} ions (curves 1 and 2). However, the impedance plots indicate that the Co^{2+} ions modify the anode kinetics in the presence of Mn^{2+} ions. For example, the difference is illustrated in Figure 5: the capacitive loop apparent between 1 and 0.1 Hz in plot (b), has disappeared in plot (a) obtained with 10 mg dm^{-3} Co^{2+}. Consequently, cobalt alters the inhibition process taking place on the lead–silver anodes.

In addition the curves $R_t i(E)$, presented in Figure 6, also show that the charge transfer resistance for oxygen evolution on lead–silver alloy anodes is reduced by the presence of Co^{2+} ions. Curves 1 and 2 show two plateaus. The first, at low polarizations, corresponds to the region where the formation of oxide layers on the

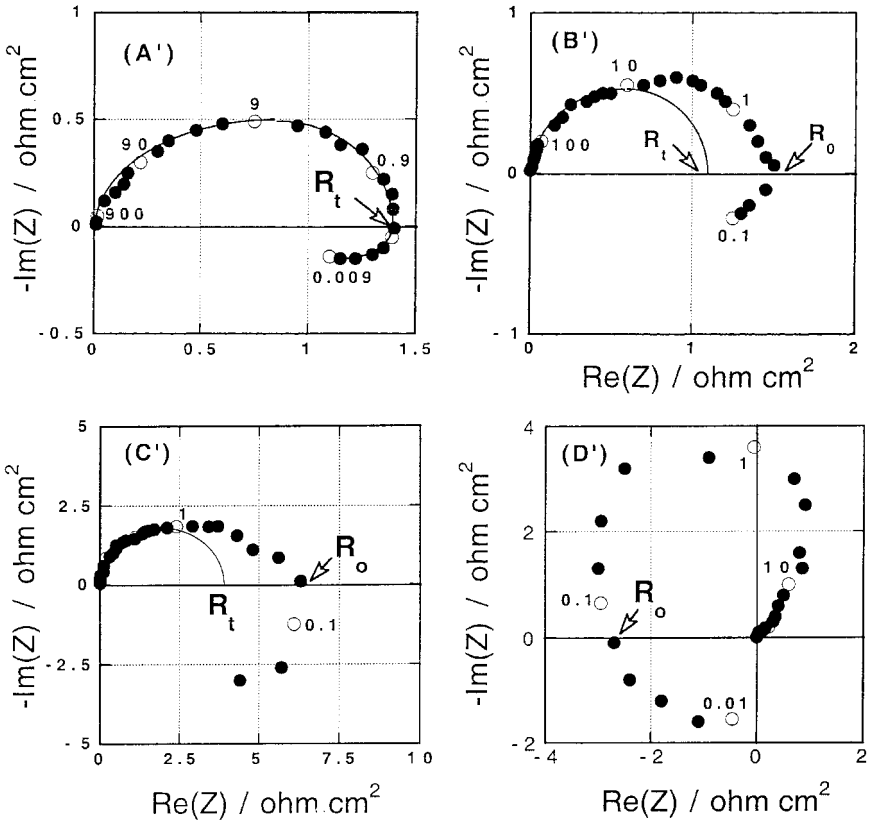

Fig. 3. Impedance plots obtained at $E = 1.355$ V in the base electrolyte (A′), and in the same electrolyte containing various concentrations of Mn^{2+} ions: (B′) 1, (C′) 5 and (D′) 10 g dm^{-3}.

electrode interferes with oxygen evolution. The second plateau at high polarizations ($E > 1.3$ V) characterizes the region where oxygen evolution predominates and indicates that this reaction follows a Tafel activation with potential. The decreased value for the plateau means that the Tafel coefficient for oxygen evolution increases in the presence of Co^{2+} ions, in agreement with the reduced polarization observed in Figure 4, curve 2.

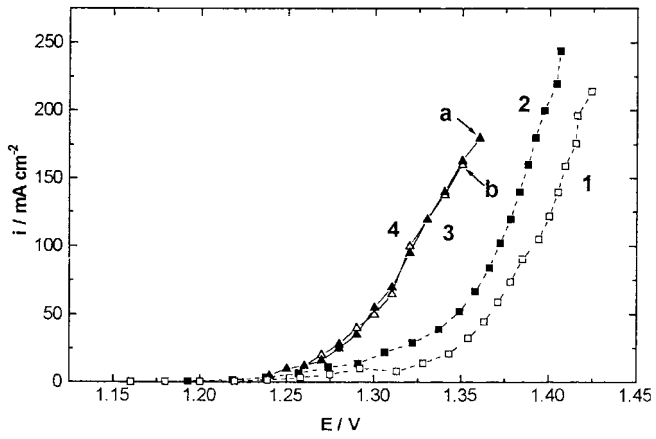

Fig. 4. Curves $i(E)$ obtained with Pb–Ag anodes in the base electrolyte (curve 1), the base electrolyte with 10 mg dm^{-3} Co^{2+} (curve 2), the base electrolyte with 5 g dm^{-3} Mn^{2+} (curve 3) and the base electrolyte with the two additives (curve 4).

In the presence of manganese, a significant increase in $R_t i$ appears over the whole potential domain, Figure 6, curves 3 and 4. Similar to the preceeding case, $R_t i$ is again reduced by Co^{2+} ions, curve 4. In spite of these opposing effects of Mn^{2+} and Co^{2+} ions on charge transfer, the reduced steady-state polarization of the electrode, curves 3 and 4 in Figure 4, does not depend on the presence of Co^{2+} and remains determined by Mn^{2+} ions.

3.2. *Case of pure lead anode*

The polarization curves, obtained with a pure lead anode and the experimental procedure previously described, are presented in Figure 7. Curve 2 shows that the influence of manganese on the oxygen overpotential on lead remains small and even decreases with increas-

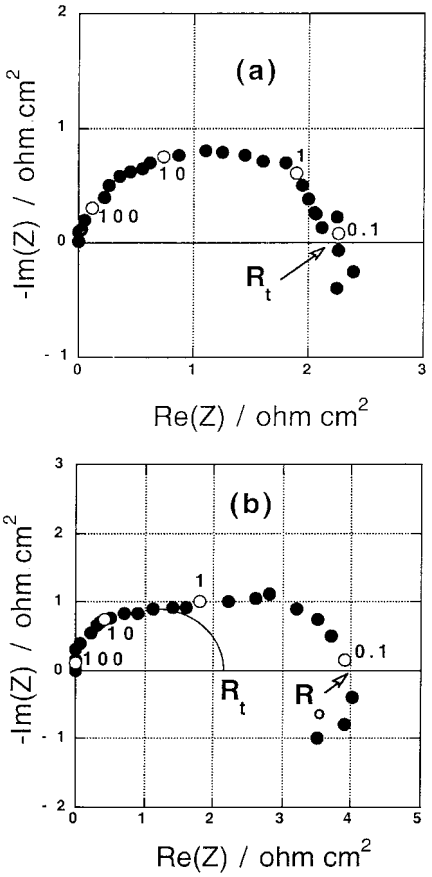

Fig. 5. Impedance plots obtained at point (b) on curve 3 in Figure 4, without Co^{2+} in the H_2SO_4–$ZnSO_4$–$MnSO_4$ electrolyte, and at point (a) on curve 4 with 10 mg dm^{-3} Co^{2+}.

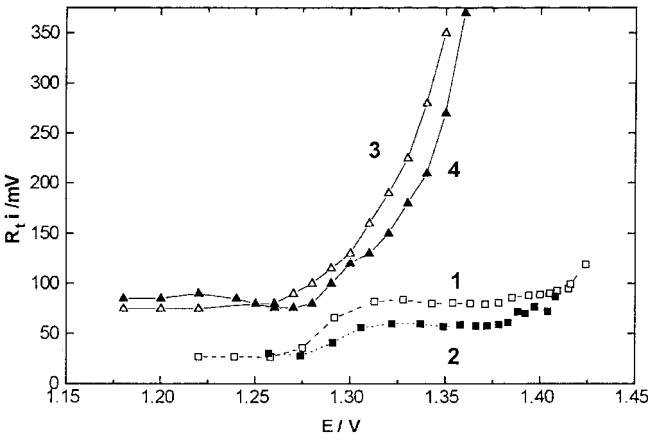

Fig. 6. Curve $R_t i(E)$ obtained for the Pb–Ag anodes in the base electrolyte (curve 1), the base electrolyte with 10 mg dm^{-3} Co^{2+} (curve 2), the base electrolyte with 5 g dm^{-3} Mn^{2+} (curve 3) and the base electrolyte with the two additives (curve 4).

ing potential. By contrast, curve 3 reveals a marked influence of cobalt in the whole range of potential. As compared to curve 1, a significant decrease in polarization is observed with both cobalt and manganese, curve 4: this decrease is close to 80 mV for $i = 100$ mA cm^{-2}.

At each point on the polarization curves, the electrode impedance was measured, and typical plots of the various electrolytes are presented in Figures 8 and 9. Figures 8(A) and 9(B) exemplify the shape of the impedance plots obtained along curves 1 and 2 in Figure 7. In the studied frequency domain, these plots show only the capacitive loop corresponding to the charge transfer resistance, R_t, for oxygen evolution. In contrast to the Pb–Ag anode, the presence of Mn^{2+} does not induce a transient inhibition of oxygen evolution on the pure lead anode surface.

With Co^{2+} ions, a medium-frequency capacitive loop appears, as illustrated on impedance plots (C), (D), (E) and (F), again indicating a transient inhibition of oxygen evolution, and suggesting the adsorption of a cobalt-containing species taking place at the relatively high polarization of lead anodes. This species probably alters the catalytic properties of the active centers involved in the oxygen evolution reaction [30]. Figure 8(C) shows that the anode behaviour is also modified at the beginning of the electrode polarization where the presence of a low-frequency feature indicates that Co^{2+} ions interfere with the growth of oxide layers on the anode.

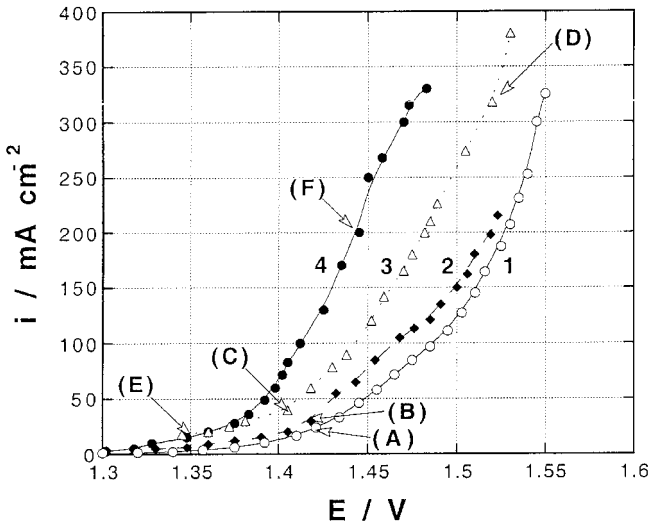

Fig. 7. Curves $i(E)$ obtained with pure lead anodes in different electrolytes: base electrolyte (curve 1), base electrolyte with 5 g dm^{-3} Mn^{2+} (curve 2), base electrolyte with 10 mg dm^{-3} Co^{2+} (curve 3), and base electrolyte with the two additives (curve 4).

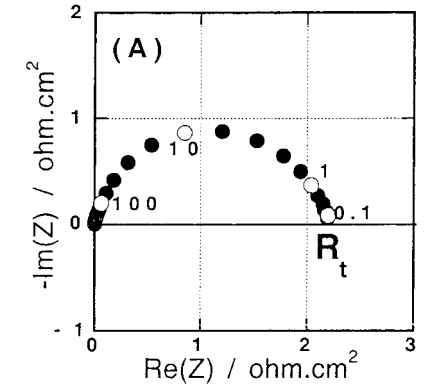

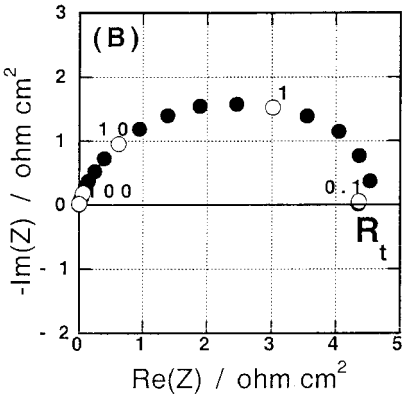

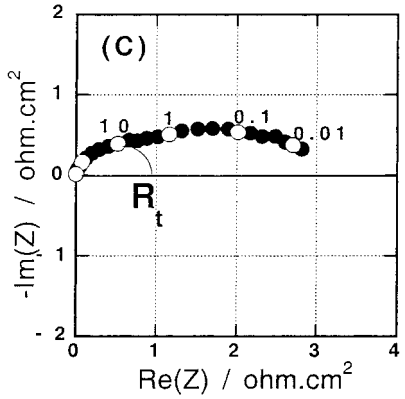

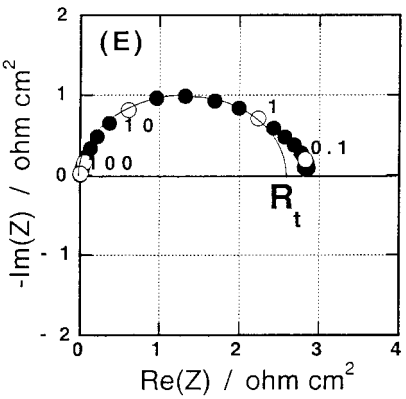

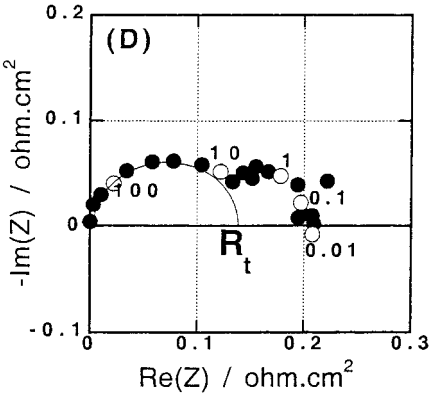

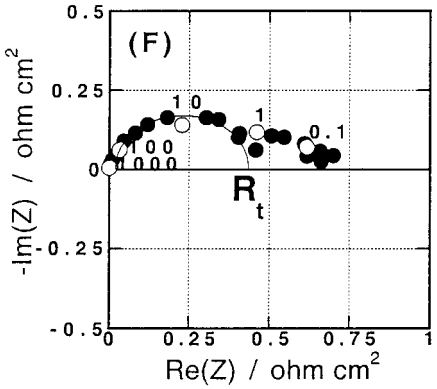

Fig. 8. Characteristic impedance plots, obtained along the $i(E)$ curves of Figure 7, with a pure lead anode polarized in the base electrolyte (A), and in the base electrolyte with 10 mg dm^{-3} Co^{2+} ions ((C) and (D)).

Fig. 9. Characteristic impedance plots, obtained along the $i(E)$ curves of Figure 7, with a pure lead anode polarized in the H_2SO_4–$ZnSO_4$–$MnSO_4$ electrolyte (B), and in the same electrolyte with 10 mg dm^{-3} Co^{2+} ions ((E) and (F)).

The variation of the $R_t i$ product as a function of the anode potential is shown in Figure 10, for each electrolyte. Two potential domains can be distinguished for the action of Co^{2+} and Mn^{2+} ions. At low polarization, i.e. below $E_1 = 1.4$ V for Mn^{2+}-containing electrolytes (curves 2 and 4) and below $E_2 = 1.43$ V for Mn^{2+}-free electrolytes (curves 1 and 3) where the formation of the oxide layers occurs simultaneously with oxygen evolution, a catalytic effect of Co^{2+} ions with a decrease in $R_t i$ values is observed. At high polarization where oxygen evolution predominates, i.e. above E_1 and E_2, $R_t i$ is potential-independent in the Mn^{2+}-free electrolytes

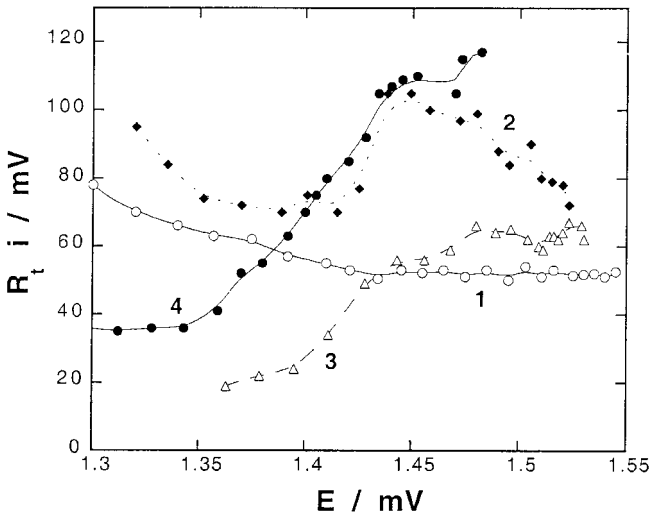

Fig. 10. Curves $R_t i(E)$ obtained with pure lead anodes in different electrolytes: base electrolyte (curve 1), base electrolyte with 5 g dm^{-3} Mn^{2+}(curve 2), base electrolyte with 10 mg dm^{-3} Co^{2+} (curve 3), and base electrolyte with the two additives (curve 4).

(curves 1 and 3), which indicates that the oxygen evolution reaction follows a Tafel activation with potential, similar to the case of lead–silver anodes. In this potential domain, the influence of Co^{2+} ions on $R_t i$ is weak, and the influence of Mn^{2+} ions becomes prevalent to produce an increased $R_t i$ product (curves 2 and 4). With the two additives, the potential dependence of $R_t i$ in Figure 10, curve 4, appears to be determined by the presence of Mn^{2+} ions and similar to the situation observed for lead–silver anodes, although higher values of $R_t i$ were obtained in Figure 6, curve 4.

It is also noteworthy that the maximum decrease in overpotential for oxygen evolution, observed with the two additives in Figure 7, appears precisely under conditions favouring both a relatively high value of $R_t i$, Figure 10, and a marked transient inhibition, Figure 9(F). Consequently, the results obtained with the pure lead anode indicate that the transient inhibition by Co^{2+} ions is basically different from the catalytic effect of these ions on the steady-state current. A catalytic influence of Mn^{2+} and Co^{2+} ions on the rate constant of oxygen evolution seems to be the determining factor for the decrease in the anode potential, which is able to supplant both a decrease in the Tafel coefficient of charge transfer and the transient inhibition generated by the cobalt-containing adsorbate.

Comparing the polarization curves in Figures 4 and 7 reveals different behaviours of cobalt and manganese. On the lead–silver alloy, the decrease in oxygen overpotential essentially results from the presence of manganese. In this case, oxygen evolves on the MnO_2 layer whose reactivity or conductivity is probably activated by silver inclusions. On a pure lead anode, the maximal decrease in overpotential results from the combined influence of manganese and cobalt. In this second case, MnO_2 alone on the electrode surface is not sufficient to catalyse oxygen evolution, and it necessitates the presence of a cobalt oxide, possibly CoO_2, to produce a catalytic effect [17].

4. Conclusion

The kinetics of lead and lead–silver anodes are modified in the presence of Mn^{2+} ions in the electrolyte. With increasing Mn^{2+} concentration, a stimulation of the steady-state current of oxygen evolution is observed, attaining a saturation limit when the Mn^{2+} concentration exceeds 5 g dm^{-3}. This catalytic effect essentially results from the stimulation of the rate constant for oxygen evolution. In the particular case of lead–silver anodes, impedance data also reveal a transient inhibition of the oxygen reaction apparent under the form of a medium-frequency capacitive feature which becomes more important with increasing Mn^{2+} concentration. This inhibition has been ascribed to the adsorption of a silver-salt containing manganese.

The influence of Co^{2+} ions on the anode kinetics has been studied both in the absence and in the presence of Mn^{2+} ions. Under steady-state conditions, the addition of Co^{2+} reduces the electrode polarization, mainly for the pure lead anode, and also a little for the lead–silver anode. With the lead–silver anodes, the presence of Co^{2+} ions also decreases the product of the charge transfer resistance R_t and current density i, thus indicating that the catalytic effect of Co^{2+} ions implies the stimulation of the Tafel coefficient of the oxygen reaction. By contrast, this coefficient is little affected by Co^{2+} ions in the case of the pure lead anode. In addition it has been shown that the medium-frequency capacitive feature is reduced on lead–silver anodes by Co^{2+} ions, whereas it is favoured on pure lead anodes whose polarization is higher. It is concluded that a cobalt-containing species adsorbs on the anode surface in competition with the silver-salt adsorbate.

On both types of electrode, pure lead and silver–lead alloy, it is shown that the maximal decrease in overpotential for oxygen evolution, attained in the presence of Co^{2+} and Mn^{2+} ions, coexists with a relatively high $R_t i$ product and a marked transient inhibition process. It consequently appears that the determining effect of Co^{2+} and Mn^{2+} ions lies in the generation of active sites able to stimulate the rate constant of oxygen evolution.

Silver in the electrode material also participates in the formation of these activated sites.

Acknowledgements

Financial support, supplied by Union-Minière (France), is gratefully acknowledged.

References

1. H. Fukubayashi, T.J. O'Keefe and W.C. Clinton, US Bureau of Mines, Washington, RI 7966 (1974).
2. D.R. Fosnacht and T.J. O'Keefe, *J. Appl. Electrochem.* **10** (1980) 495.
3. D.R. Fosnacht and T.J. O'Keefe, *Met. Trans. B* **14B** (1983) 645.
4. M. Maja, *Electrochim. Met.* **4** (1967) 469.
5. M. Maja and S. Pozzoli, *La Chimica e l'Industria* **51** (1969) 133.
6. M. Maja, N. Penazzi, R. Fratesi and G. Roventi, *J. Electrochem. Soc.* **129** (1982) 2695.
7. M. Maja, N. Penazzi, R. Fratesi and G. Roventi, *Oberfläche Surfa.* **24** (1983) 234.
8. D.J. Mackinnon, R.M. Morrison and J.M. Brannen, *J. Appl. Electrochem.* **16** (1986) 53.
9. D.J. Mackinnon, J.M. Brannen and P.L. Fenn, *J. Appl. Electrochem.* **17** (1987) 1129.
10. A.R. Ault and E.J. Frazer, *J. Appl. Electrochem.* **18** (1988) 583.
11. I.W. Wark, *J. Appl. Electrochem.* **9** (1979) 721.
12. C. Bozhkov, M. Petrova and St. Rashkov, *J. Appl. Electrochem.* **22** (1992) 73.
13. Ts. Dobrev, C. Cachet and R. Wiart, *J. Appl. Electrochem.* **28** (1998) 1195
14. P. Ramachandran and K. Balakrishnan, *Bull. Electrochem.* **6** (1990) 455.
15. G.Z. Kiryakov and V.V. Stender, *Zh. Prikl. Khim.* **25** (1952) 23.
16. K. Hein, I. Duman and S. Timur, *Metallwiss. Technik* **48** (1994) 532.
17. O. Forsen, J.J. Kukkonen, J. Aromaa and S. Ylassari, European seminar *Improved Technologies for the Rational Use of Energy in the Non-ferrous Industry in Europe*, Milan, Italy (Nov. 1992), *Proceedings*, p. 125.
18. R.C. Villas Bôas, *Synergetic Phenomena in Zinc Electrowinning*, NSF/CNPq, Rio de Janeiro (1977).
19. D. Pavlov and T. Rogachev, *Electrochim. Acta* **31** (1986) 241.
20. F. Hine, Y. Ogata and M. Yasuda *Bull. Electrochem.* **4** (1988) 61.
21. R. Mraz, R.M. Vaclav and S. Tichy, *Electrochim. Acta* **18** (1973) 551.
22. E.R. Cole and T.J. O'Keefe, US Bureau of Mines, PGH, PA 25270, US Government Printing Office (1981).
23. D. Buttinelli, G. D'Angelo and G. Signorelli, *Industria Mineraria*, (March) (1974) 118.
24. R.H. Newham, *J. Appl. Electrochem.* **22** (1992) 116.
25. C. Rerolle, These de Doctorat, Université P. et M. Curie, Paris (1994).
26. C. Rerolle and R. Wiart, *Electrochim. Acta* **40** (1995) 939.
27. C. Cachet, C. Rerolle and R. Wiart, *Electrochim. Acta* **41** (1996) 83.
28. C. Rerolle and R. Wiart, *Electrochim. Acta* **41** (1996) 1063.
29. C. Cachet, C. Le Pape-Rerolle and R. Wiart, *J. Appl. Electrochem* **28** (1998) 193.
30. D. Pavlov and B. Monahov, *J. Electrochem. Soc.* **145** (1998) 70.